Numerical simulation and Scientific Computing II – Fluid mechanics. General informations:

- **Submission is due on Thursday, May** 18^{th} **2023, 23:59**. Please upload the material in TUWEL.
- Include the name of all group members (max. 3) in your submission
- Submit everything (source files, results, animations – if any – and final reports) as one zip-file per exercise. Include a README file to explain the content and the usage of the different files in the archives.
- The number of points corresponding to each task of the exercises is indicated within square brackets, e.g. [2 POINTS]
- You can write your codes in Fortran, Matlab, Python, C/C++. Note: assistance can be given in case you use Fortran or Matlab.
- In case you are willing to use Matlab to solve the exercises, but you do not have it already installed in your computer, then you can download and install it via the following link: http://www.sss.tuwien.ac.at/sss/mla/. There is a free Matlab version for TU students.

Exercise 1: Numerical solution of the diffusion equation in a finite domain

Consider the 1D unsteady diffusion equation in cartesian coordinates:

$$\frac{\partial C}{\partial t} = D\frac{\partial^2 C_i}{\partial x^2}, \tag{1}$$

with $D = 10^{-6}$ the binary diffusion coefficient. The size of the domain along x is h (i.e. the domain is characterized by a finite length). The grid spacing is Δx (obtained discretizing the domain length h using N_x points), and the time step is Δt. Initial condition is $C = 0$ everywhere inside the domain.

Questions

1. Assume Dirichlet/Neumann boundary conditions: $C = 1$ at $x = 0$ and $\partial C/\partial x = 0$ at $x = h$. Solve Eq. 1 by an *explicit* finite difference approach that is 2^{nd} order accurate in space and 1^{st} order accurate in time. Compare the results with the analytical solution (see Lecture for reference). Show that the numerical solution is not unconditionally stable. In particular, show that it is unstable for $d = D\Delta t/\Delta x^2 > 0.5$. [2 POINTS]

2. Assume Dirichlet boundary conditions at both boundaries: $C = 1$ at $x = 0$ and $C = 0$ at $x = h$. Solve Eq. 1 for the same cases and using the same discretization strategy (i.e. *explicit* finite difference approach, 2^{nd} order in space and 1^{st} order in time) analyzed at point 1. Compare the long term behavior, $\lim_{t\to\infty} C(x)$, of the present case with that of the previous case, point 1. [2 POINTS]

3. Assume Dirichlet/Neumann boundary conditions: i.e. $C = 1$ at $x = 0$ and $\partial C/\partial x = 0$ at $x = h$. Solve the equation using an *implicit* scheme (2^{nd} order in space and 1^{st} order in time) and discuss the stability of the solution. Compare the new results with those obtained at point 1. [2 POINTS]

4. Assume Dirichlet/Neumann boundary conditions: i.e. $C = 1$ at $x = 0$ and $\partial C/\partial x = 0$ at $x = h$. Solve the equation using an *implicit* scheme that is 2^{nd} order in space and $2nd$ order in time. Discuss the accuracy of the solution in comparison with that obtained at point 3. [2 POINTS]

Produce plots and movies to support your conclusions (for your convenience, you can take plots and movies presented during the lecture as reference for the purpose).

Exercise 2: Numerical solution of the linear advection equation in a periodic domain

Consider the 1D linear advection equation in cartesian coordinates:

$$\frac{\partial C_i}{\partial t} = U \frac{\partial C_i}{\partial x}, \tag{2}$$

where $U = 1$ is a given convection velocity. Assume $\Delta x = 0.01$.

Questions

1. Solve Eq. 2 with the *upwind* scheme (please refer to the lecture for details). Assume two different initial conditions: a square pulse ($C = 1$ for $0.1 < x < 0.3$, $C = 0$ elsewhere) and a Gauss signal (for example $C = \exp(-10(4x - 1)^2)$). The shape of these initial conditions is given in Fig. 1. Discuss the stability and accuracy of the solution for varying Courant number Co. In particular, what happens for $Co > 1$? And for $Co < 1$? And for $Co = 1$? [2 POINTS]

Produce plots and movies to support your conclusions (for your convenience, you can take plots and movies presented during the lecture as reference for the purpose).

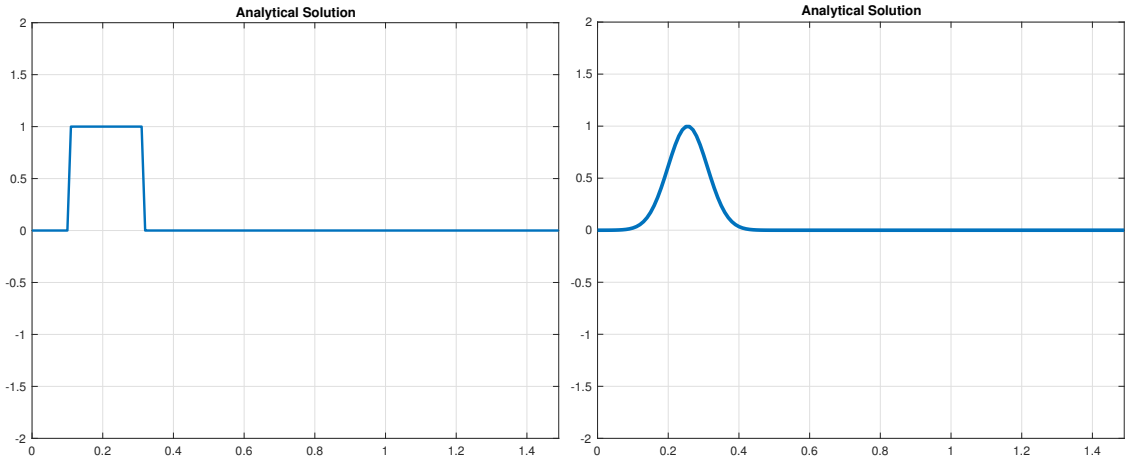

Figure 1: Initial condition for the linear advection equation: square pulse (left), Gauss signal (right).

Exercise 3: Numerical solution of the lid-driven cavity flow in a 2D cartesian domain

Consider the flow inside a rectangular domain (cartesian coordinates), as sketched in Fig.2. The governing balance equations for the problem (continuity, Navier-Stokes and scalar transport) are:

$$\frac{\partial u_i}{\partial x_i} = 0 \tag{3}$$

$$\frac{\partial u_i}{\partial t} + u_j \frac{\partial u_i}{\partial x_j} = -\frac{\partial p}{\partial x_i} + \frac{1}{Re} \frac{\partial^2 u_i}{\partial {x_j}^2} \tag{4}$$

$$\frac{\partial C}{\partial t} + u_j \frac{\partial C}{\partial x_j} = \frac{1}{RePr} \frac{\partial^2 C}{\partial {x_j}^2} \tag{5}$$

where u_i is the flow velocity, p is pressure, C is the scalar concentration while Re and Pr are the Reynolds and Prandtl numbers, respectively (main flow parameters[1]). Boundary conditions are given in Fig.2.

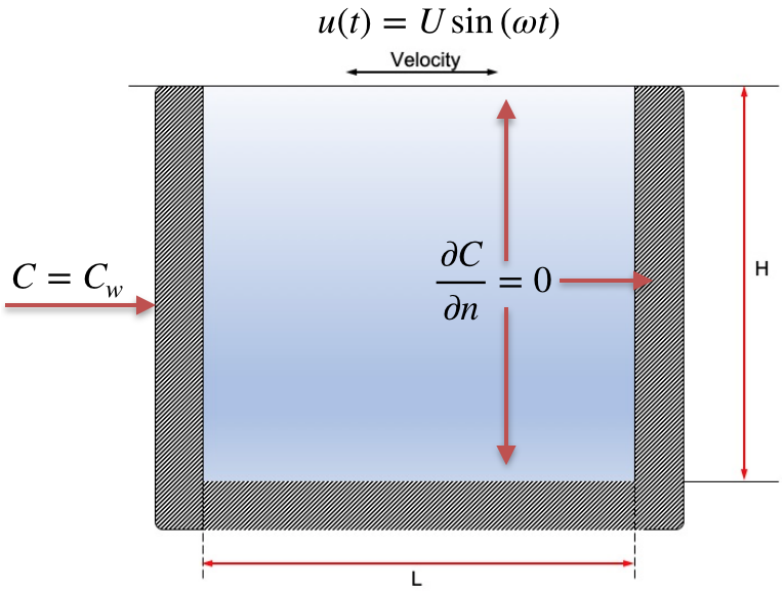

Figure 2: Sketch of the flow configuration with indication of the boundary conditions.

[1] For scalar transport, the Schmidt number (Sc) is more commonly introduced instead of the Prandtl number (Pr, used only when the transported scalar is temperature transport). In the present context, and to simplify notation, we assume $Sc = Pr$.

Questions

1. Rewrite the above system of equations, Eq. 3-5, using the $\psi - \omega$ formulation (please refer to the lecture for details). Solve the obtained system of equations by an *explicit* finite difference approach that is 2^{nd} order accurate in space and 1^{st} order accurate in time. To define appropriate boundary conditions for the $\psi - \omega$ formulation, please refer to the lecture. Consider a constant velocity $u(t) = U = 1$ at the upper boundary, and set $C = C_w = 1$ at the left boundary. Assume $H = L = 1$, and discretize the domain using $N_x = N_y = 100$ grid points along x and y. Use a time step $\Delta t = 10^{-3}$. Initial conditions are $\psi = 0, \omega = 0, C = 0$ everywhere inside the domain. Run the simulation until a *steady-state condition* is reached. This condition can be assessed by looking at the behavior of the vorticity field ω. In particular, the flow can be considered steady when, in each grid point, $|\omega_{i,j}^{n+1} - \omega_{i,j}^{n}| < \epsilon$, with $\epsilon = 10^{-6}$ (which means that the value of the vorticity at the new time instant does not differ significantly from the value at the previous time instant). Plot the behavior of the stream function for $Pr = 1$, and for varying Reynolds number in the range $100 < Re < 1000$ (simulations at Re>1000 are more demanding in terms of computational time, hence not required). Compare your results with those shown in Fig. 3.
   Note: further details on the cavity flow problem, and on its numerical solution, can be found in Fletcher, C.A.J, *Computational techniques for fluid dynamics – 2 volume* (1991), Springer-Verlag Berlin Heidelberg (the relevant section of this book, Chapter 17.3, pag. 373-379, has been included at the end of this document). [+2 ADDITIONAL POINT]

2. Assume now a periodic velocity, $u(t) = \sin(\omega t)$, at the upper boundary. The Reynolds number is equal to $Re = 2000$. Consider different values of ω: $\omega = 1/3$, $\omega = 1/2$, $\omega = 3/4$. Initial conditions are as in point 1. Plot the behavior of the concentration in time (possibly an animation, see lecture). [+1 ADDITIONAL POINT]

Produce plots and movies to support your conclusions (for your convenience, you can take plots and movies presented during the lecture as reference for the purpose).

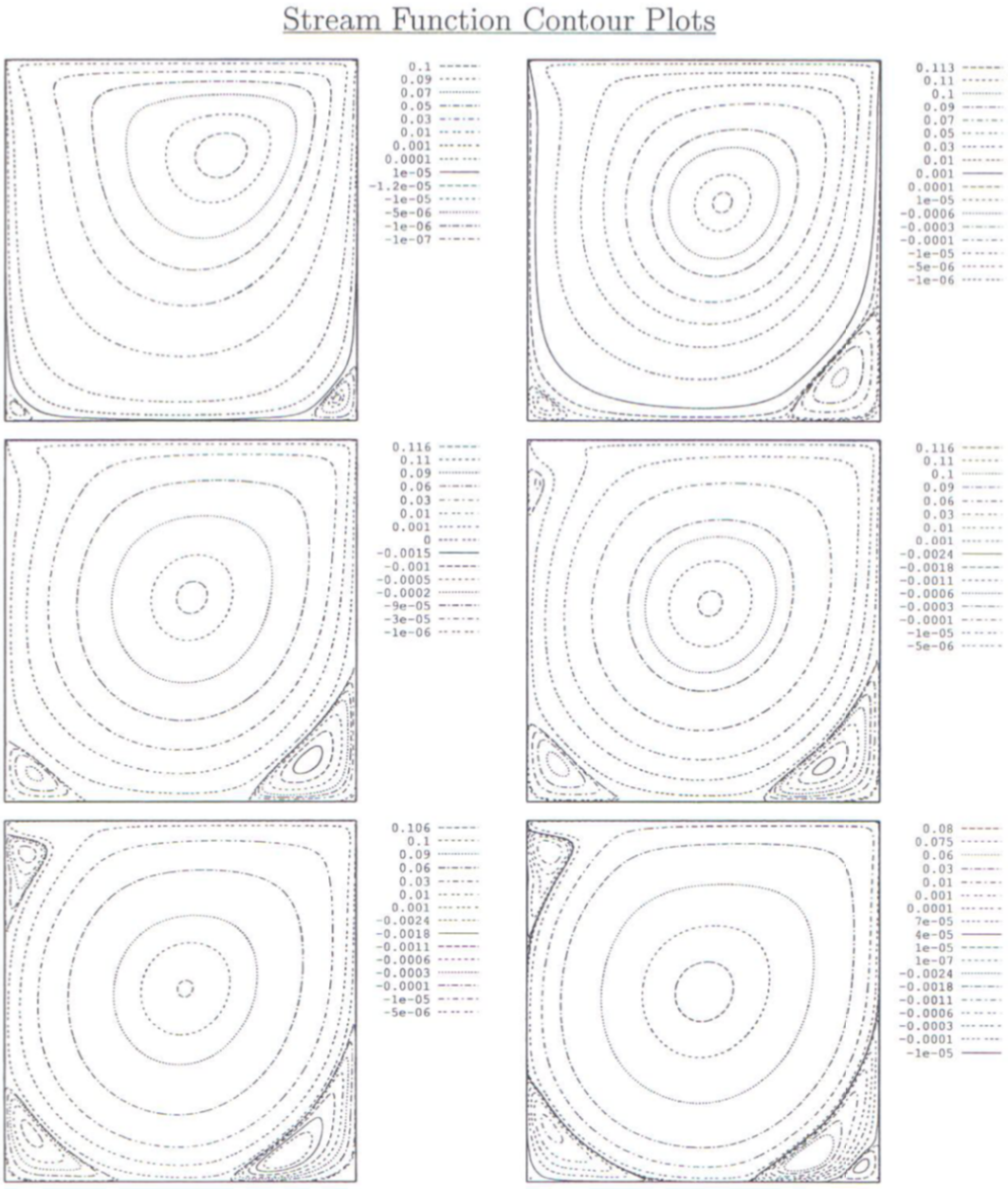

Figure 3: Reference results for the streamfuction in the cavity flow problem (required for point 1). First row, $Re = 100$ (left) and $Re = 400$ (right). Second row, $Re = 1000$ (left) and $Re = 2000$ (right). Third row, $Re = 5000$ (left) and $Re = 7500$ (right).

mixed interpolation (u, v, p) formulation. For quadratically-interpolated velocity on elements with curved sides (to suit irregular geometries) the consistent penalty function formulation is more accurate (Engelman et al. 1982) than the use of reduced integration and theoretically better supported.

The finite element method lends itself to the construction of general-purpose codes for solving coupled fluid flow, heat transfer problems in complicated geometric domains. FIDAP (Fluid Dynamic Analysis Program) is such a general-purpose code and is described by Engelman (1982). A representative problem that can be successfully modelled by FIDAP is indicated in Fig. 17.11.

A conduit passing through a wing fuel tank contains three electrical wires at different temperatures. FIDAP determines the natural convection in the air gap surrounding the wires. Shown in Fig. 17.11 are the finite element grid, temperature contours, velocity vectors and streamlines for a Rayleigh number of 800 000. The solution indicates thermal plumes rising from the hot wire and dropping from the cold wire. The grid contains 2654 nodes and 624 nine-node quadrilateral elements.

17.3 Vorticity, Stream Function Variables

As an alternative to solving the governing equations in primitive variables it is possible to avoid the explicit appearance of the pressure by introducing the vorticity and stream function as dependent variables (Sect. 11.5.1), at least in two dimensions.

In two-dimensional flow the vorticity vector

$$\boldsymbol{\zeta} = \text{curl}\, \mathbf{q} \tag{17.88}$$

has a single component, which is defined conventionally as

$$\zeta = \frac{\partial u}{\partial y} - \frac{\partial v}{\partial x} \,. \tag{17.89}$$

The transport equation for the vorticity (11.85) with the aid of the continuity equation (17.1) is

$$\frac{\partial \zeta}{\partial t} + \frac{\partial (u\zeta)}{\partial x} + \frac{\partial (v\zeta)}{\partial y} - \frac{1}{\text{Re}} \left(\frac{\partial^2 \zeta}{\partial x^2} + \frac{\partial^2 \zeta}{\partial y^2} \right) = 0 \,, \tag{17.90}$$

where the Reynolds number $\text{Re} = U_\infty L/\nu$. In two dimensions a stream function can be defined by

$$u = \frac{\partial \psi}{\partial y} \quad \text{and} \quad v = -\frac{\partial \psi}{\partial x} \,, \tag{17.91}$$

and substitution into (17.89) produces the following Poisson equation for the stream function:

$$\frac{\partial^2 \psi}{\partial x^2} + \frac{\partial^2 \psi}{\partial y^2} = \zeta \ . \tag{17.92}$$

Equations (17.90–92) constitute the governing equations for the vorticity stream function formulation of incompressible laminar flow. Strictly by substituting (17.91) into (17.90) it is possible to eliminate the explicit appearance of u and v. However, such a formulation may produce less accurate solutions although it does save the additional storage of u and v. Initial and boundary conditions to suit (17.90–92) are discussed in Sect. 11.5.1.

The system of equations (17.90–92) is applicable to both steady and unsteady laminar viscous flow. However, only the vorticity transport equation (17.90) depends explicitly on time. Consequently, for unsteady problems (17.92) implies that the stream function field must be determined to be compatible with the time-dependent vorticity distribution at every time-step.

For unsteady problems (17.90) is parabolic in time if u and v are known. Thus it can be marched efficiently in time using an ADI or approximation factorisation technique (Sect. 8.2). At each time step the discrete form of (17.92) is solved for ψ. Equation (17.92) is strongly elliptic if ζ is known and can be solved by iterative (Sect. 6.3) or direct methods (Sect. 6.2). Since (17.92) is a Poisson equation very efficient direct methods (Sect. 6.2.6) are available if the grid is uniform.

For steady flow problems, (17.91, 92) and the steady form of (17.90) are a system of elliptic partial differential equations. Since (17.90) is nonlinear it is necessary to employ an iterative algorithm. At each step of the iteration (17.90 and 92) are used to update the ζ and ψ solutions either sequentially or as a coupled system. Gupta and Manohar (1979) employ a sequential algorithm.

It is necessary to use under-relaxation in determining boundary values of the vorticity, to provide a Dirichlet boundary condition for the steady form of (17.90). The cause of this problem is that physical boundary conditions are available on ψ and $\partial\psi/\partial n$ but none on ζ. When numerical boundary conditions are constructed for ζ which satisfy the integral boundary condition (11.90), no under-relaxation is required (Quartapelle and Valz-Gris 1981), even though a sequential algorithm is used.

However, if the steady form of (17.90 and 92) are solved as a coupled system the two boundary conditions on ψ and $\partial\psi/\partial n$ are sufficient. Campion-Renson and Crochet (1978) use such a formulation with a finite element method to examine the flow in a driven cavity. No numerical boundary condition for ζ is required.

The pseudotransient strategy (Sect. 6.4) offers an alternative path to obtain the steady flow solution. To implement the pseudotransient approach (17.92) is replaced by

$$\frac{\partial \psi}{\partial \tau} - \left\{ \frac{\partial^2 \psi}{\partial x^2} + \frac{\partial^2 \psi}{\partial y^2} - \zeta \right\} = 0 \ . \tag{17.93}$$

When the steady state is reached (17.93) reverts to (17.92). The choice of the time-step $\Delta\tau$ that appears after discretisation of (17.93) provides an additional level of control over the pseudotransient iteration. The sequential versus coupled treatment of (17.90 and 93) is also relevant to the pseudotransient strategy. Typical examples are provided in the next section.

17.3.1 Finite Difference Formulations

In this section we consider a typical sequential and a typical coupled solution algorithm for the steady laminar flow in a driven cavity (Fig. 17.12). The lid of the cavity moves continuously to the right with a velocity $u=1$. No-slip boundary conditions on the velocity components u and v are equivalent, through (17.91), to the indicated boundary conditions on ψ and $\partial\psi/\partial n$.

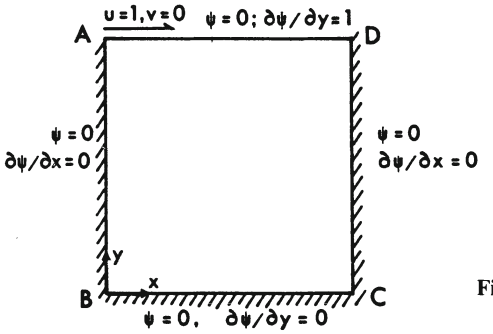

Fig. 17.12. Two-dimensional driven cavity

A sequential algorithm due to Mallinson and de Vahl Davis (1973) is described which is based on a pseudotransient solution of (17.90 and 93). In this formulation uniform-grid three-point centred difference formulae are introduced for first and second spatial derivatives. In the notation of Chap. 8,

$$\frac{\partial(u\zeta)}{\partial x}=L_x(u\zeta)_{j,k}+O(\Delta x^2)\ , \quad \frac{\partial^2\zeta}{\partial y^2}=L_{yy}\zeta_{j,k}+O(\Delta y^2)\ , \quad \text{etc.},$$

where

$$L_x(u\zeta)_{j,k}=\frac{(u\zeta)_{j+1,k}-(u\zeta)_{j-1,k}}{2\Delta x}\ , \quad \text{and} \tag{17.94}$$

$$L_{yy}\zeta_{j,k}=\frac{\zeta_{j,k-1}-2\zeta_{j,k}+\zeta_{j,k+1}}{\Delta y^2}\ .$$

Mallinson and de Vahl Davis write the semi-discrete form of (17.90) as

$$\frac{1}{\varepsilon}\frac{\partial\zeta_{j,k}}{\partial t}=(A^x+A^y)\zeta_{j,k}\ , \quad \text{where} \tag{17.95}$$

$$A^x\zeta_{j,k}=(1/\mathrm{Re})L_{xx}\zeta_{j,k}-L_x(u\zeta)_{j,k}\ ,$$

$$A^y\zeta_{j,k}=(1/\mathrm{Re})L_{yy}\zeta_{j,k}-L_y(v\zeta)_{j,k}\ ,$$

and ε is a relaxation parameter that can be varied spatially. When all grid points are considered the following vector equation results:

$$\frac{\partial \boldsymbol{\zeta}}{\partial t} = \varepsilon [\underline{\boldsymbol{A}}^x + \underline{\boldsymbol{A}}^y] \boldsymbol{\zeta} \ . \tag{17.96}$$

The elements of the matrices $\underline{\boldsymbol{A}}^x$ and $\underline{\boldsymbol{A}}^y$ can be obtained from (17.94).

Equation (17.96) and an equivalent semi-discrete vector equation, based on (17.93), are advanced in time using an algorithm introduced by Samarskii and Andreev (1963),

$$\begin{aligned} &[I - 0.5\varepsilon\, \Delta t\, \underline{\boldsymbol{A}}^x] \Delta \boldsymbol{\zeta}^* = \varepsilon \Delta t [\underline{\boldsymbol{A}}^x + \underline{\boldsymbol{A}}^y] \boldsymbol{\zeta}^n \ , \\ &[I - 0.5\varepsilon\, \Delta t\, \underline{\boldsymbol{A}}^y] \Delta \boldsymbol{\zeta}^{n+1} = \Delta \boldsymbol{\zeta}^* \quad \text{and} \\ &\boldsymbol{\zeta}^{n+1} = \boldsymbol{\zeta}^n + \Delta \boldsymbol{\zeta}^{n+1} \ . \end{aligned} \tag{17.97}$$

It is clear that (17.97) is equivalent to (8.23 and 24) with $\beta = 0.5$ and the u and v terms in $\underline{\boldsymbol{A}}^x$, $\underline{\boldsymbol{A}}^y$ evaluated at time-level n. This is essentially an approximate factorisation with Crank–Nicolson time differencing. A consideration of the modified Newton method (Sects. 6.4 and 10.4.3) suggests that setting $\beta = 1$ would produce a more rapid convergence to the steady state.

Mallinson and de Vahl Davis apply the Samarskii and Andreev scheme sequentially to (17.93 and 90). They find that the fastest convergence corresponds to $\Delta t \approx 0.8 \Delta x^2 = 0.8 \Delta y^2$ and $\Delta \tau \approx 50 \varepsilon \Delta t$. De Vahl Davis and Mallinson (1976) use this algorithm to compare three-point central differencing and two-point upwind differencing for the convective terms in (17.90) for large Reynolds numbers. Clearly the higher-order upwind schemes (Sects. 9.3.2 and 17.1.5) could be incorporated into the present method with some modification of the implicit algorithm.

When solving (17.93) for the driven cavity problem the Dirichlet boundary condition for ψ is used. When solving (17.90) a Dirichlet boundary condition for ζ is constructed. How this is done is indicated in Sect. 17.3.2.

Rubin and Khosla (1981) solve (17.90 and 92) as a coupled system using a modified strongly implicit procedure (Sect. 6.3.3). To obtain a diagonally dominant system of coupled equations for large values of Re the following discretisation of $\partial(u\zeta)/\partial x$ is introduced:

$$\frac{\partial (u\zeta)}{\partial x} \approx \mu_x L_x^+ (u\zeta)_{j,k}^{n+1} + (1 - \mu_x) L_x^- (u\zeta)_{j,k}^{n+1} + 0.5 \Delta x (1 - 2\mu_x) L_{xx} (u\zeta)_{j,k}^n \ , \tag{17.98}$$

where

$$L_x^+ (u\zeta)_{j,k} = \frac{[(u\zeta)_{j+1,k} - (u\zeta)_{j,k}]}{\Delta x} \ , \qquad L_x^- (u\zeta)_{j,k} = \frac{[(u\zeta)_{j,k} - (u\zeta)_{j-1,k}]}{\Delta x} \ ,$$

and $\mu_x = 0$ if $u_{j,k} \geqq 0$ and $\mu_x = 1$ if $u_{j,k} < 0$. The above scheme due to Khosla and Rubin (1974) is an upwind scheme at the implicit level $(n+1)$. However, under steady-state conditions it reverts to a three-point centred finite difference scheme.

Using (17.98) and an equivalent form for $\partial(v\zeta)/\partial y$, but assuming $u, v > 0$, the discrete form of (17.90 and 92) can be written

$$\frac{\zeta_{j,k}^{n+1}}{\Delta t} + L_x^-(u\zeta)_{j,k}^{n+1} + L_y^-(v\zeta)_{j,k}^{n+1} - \frac{1}{\mathrm{Re}}\{L_{xx}+L_{yy}\}\zeta_{j,k}^{n+1}$$

$$= \frac{\zeta_{j,k}^{n}}{\Delta t} - 0.5\Delta x\, L_{xx}(u\zeta)_{j,k}^{n} - 0.5\Delta y\, L_{yy}(v\zeta)_{j,k}^{n} \ , \tag{17.99}$$

$$\{L_{xx}+L_{yy}\}\psi_{j,k}^{n+1} - \zeta_{j,k}^{n+1} = 0 \ . \tag{17.100}$$

Equations (17.99 and 100) constitute a 2×2 system of equations which is diagonally dominant and couples together implicit $(n+1)$ values of ζ and ψ at grid points $(j-1, k)$, (j, k), $(j+1, k)$, $(j, k-1)$ and $(j, k+1)$. The velocity components in (17.99) are evaluated at the explicit (n) time level. If (17.99 and 100) at all interior nodes are considered collectively the resulting sparse 2×2 block matrix equation can be

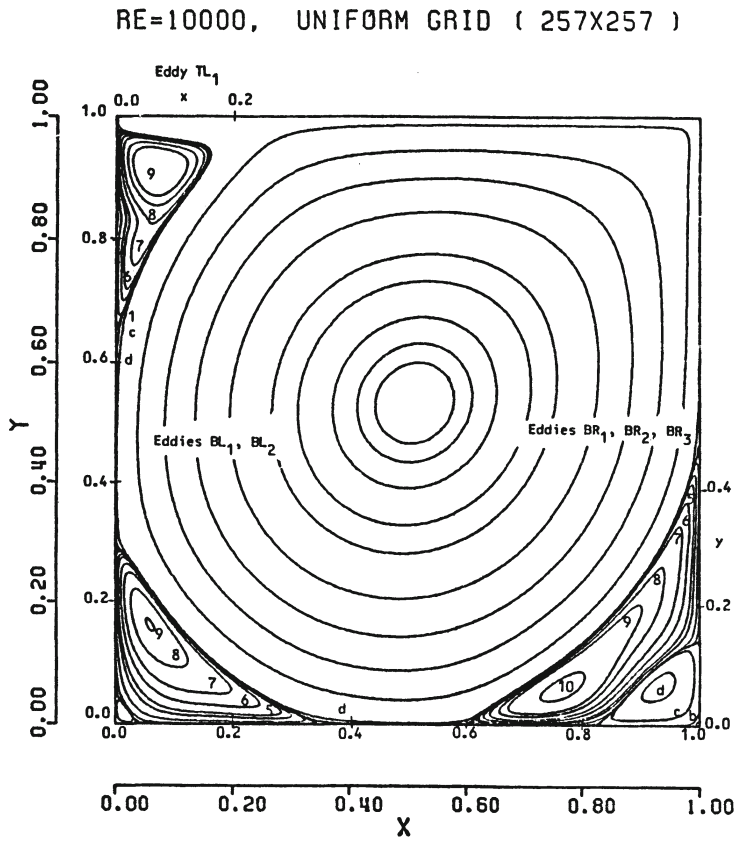

Fig. 17.13. Streamline pattern for flow in a driven cavity at Re = 10 000 (after Ghia et al., 1982; reprinted with permission of Academic Press)

solved efficiently using the strongly implicit procedure (Sect. 6.3.3). The details are provided by Rubin and Khosla (1981). Because of the strong coupling between ζ and ψ at the implicit time level no under-relaxation is required for stability when implementing the vorticity boundary condition.

Ghia et al. (1982) combine the Rubin and Khosla formulation with multigrid (Sect. 6.3.5) to obtain the flow behaviour in a driven cavity (Fig. 17.12) for Reynolds numbers up to 10000 on a 257×257 uniform grid. A typical result is shown in Fig. 17.13. The flow is characterised by a primary eddy filling most of the cavity and a sequence of counterrotating corner eddies. Ghia et al. note that the use of multigrid produces an algorithm that is about four times more efficient than using the strongly implicit procedure conventionally on the finest grid.

17.3.2 Boundary Condition Implementation

The implementation of the boundary conditions for the ζ, ψ formulation will be discussed in this section. Most attention will be given to the construction of the vorticity boundary condition at the solid surface. However, the prescription of appropriate boundary conditions at inflow and outflow boundaries is also important and will be discussed in relation to the flow past a backward-facing step.

As indicated in Fig. 17.12 the no-slip boundary conditions at a solid surface are equivalent to

$$\psi = 0 \quad \text{and} \quad \frac{\partial \psi}{\partial n} = g \ . \tag{17.101}$$

The first boundary condition is used with the Poisson equation for the streamfunction (17.92). The second boundary condition is used in the construction of a boundary condition for the vorticity. This will be illustrated for the lid (AD in Fig. 17.12). A Taylor series expansion of the streamfunction about the grid point (j, k) on AD gives

$$\psi_{j,k-1} = \psi_{j,k} - \Delta y \left[\frac{\partial \psi}{\partial y}\right]_{j,k} + \frac{\Delta y^2}{2}\left[\frac{\partial^2 \psi}{\partial y^2}\right]_{j,k} + \ldots \ . \tag{17.102}$$

From the discrete form of (17.92) and (17.101a),

$$\zeta_{j,k} = \left[\frac{\partial^2 \psi}{\partial y^2}\right]_{j,k} , \tag{17.103}$$

$$\psi_{j,k} = 0 \quad \text{and} \quad \left[\frac{\partial \psi}{\partial y}\right]_{j,k} = g_j \ .$$

Consequently (17.102) can be rearranged to give

$$\zeta_{j,k} = \frac{2}{\Delta y^2}(\psi_{j,k-1} + \Delta y \, g_j) + O(\Delta y) \ . \tag{17.104}$$

This first-order formula was first used by Thom (1933) and has been used extensively since. Comparable formulae can be readily obtained for the other surfaces.

Since a second-order accurate discretisation is used in the interior it is desirable to use a second-order accurate implementation of the boundary conditions (Sect. 7.3). This can be achieved as follows.

A second-order implementation of (17.103) is

$$\zeta_{j,k}=\frac{\psi_{j,k-1}-2\psi_{j,k}+\psi_{j,k+1}}{\Delta y^2}+O(\Delta y^2)\ . \tag{17.105}$$

In addition, a third-order accurate expressions for $[\partial\psi/\partial y]_{j,k}$ is

$$g_j=\left[\frac{\partial\psi}{\partial y}\right]_{j,k}=\frac{\psi_{j,k-2}-6\psi_{j,k-1}+3\psi_{j,k}+2\psi_{j,k+1}}{6\Delta y}+O(\Delta y^3)\ . \tag{17.106}$$

The nodal value $\psi_{j,k+1}$ lies outside of the computational domain and is eliminated from (17.105 and 106) to give

$$\zeta_{j,k}=\frac{0.5}{\Delta y^2}(8\psi_{j,k-1}-\psi_{j,k-2})+\frac{3g_j}{\Delta y}+O(\Delta y^2)\ . \tag{17.107}$$

This form is attributed to Jensen (1959) by Roache (1972) and is used by Pearson (1965) and Ghia et al. (1982).

Equation (17.107) produces more accurate solutions than the use of (17.104) in the comparative tests of Gupta and Manohar (1979). However, when used in a sequential algorithm more iterations are required using (17.107), and for large values of Re divergence may occur even when the boundary value of the vorticity is under-relaxed. When used in a coupled algorithm (17.107) causes no particular difficulty.

An alternative vorticity boundary condition for ζ is available in a pseudo-transient formulation,

$$\zeta_{j,k}^{n+1}=\zeta_{j,k}^{n}-\beta\{[\partial\psi/\partial n]-g\}_{j,k}\ . \tag{17.108}$$

This appears to provide a more direct implementation of the boundary condition (17.101b). The relaxation parameter β must be chosen appropriately (Israeli 1972) to ensure convergence. However, Peyret and Taylor (1983, p. 187) point out a rather direct link with a vorticity boundary value evaluation via (17.104), as follows.

At the $(n+1)$-th step of a pseudotransient formulation the boundary value for the vorticity is given by

$$\zeta_{j,k}^{n+1}=\gamma\zeta_{j,k}^{*}+(1-\gamma)\zeta_{j,k}^{n}\ , \tag{17.109}$$